J. Fluid Mech. (1989), *vol.* 202, *pp.* 339–366
Printed in Great Britain

Hydrodynamic and morphological stability of the unidirectional solidification of a freezing binary alloy: a simple model

By S. A. FORTH AND A. A. WHEELER
School of Mathematics, University of Bristol, University Walk, Bristol, BS8 1TW, UK

(Received 8 August 1988)

In this paper we consider the effect of a model boundary-layer flow on the hydrodynamic and morphological stability of a simple model of the solidification of a binary alloy. We conduct a linear analysis and develop asymptotic solutions for large Schmidt number and large Reynolds number. We also present numerical solutions for data appropriate to a lead–tin alloy. We show that for modes parallel to the free-stream velocity the flow is responsible for the appearance of travelling waves and, for common values of the material parameters, may stabilize the morphological stability of the interface. However the morphological stability of modes perpendicular to the free-stream velocity is unaffected by the presence of the flow. The hydrodynamic stability of the boundary layer is very weakly affected by the presence of the interface, which we attribute to the large Schmidt numbers associated with real crystal growth situations.

1. Introduction

The unidirectional solidification of a liquid binary alloy in the presence of an imposed temperature gradient is the main method by which electronic materials are produced. Examples of these materials are doped silicon, gallium arsenide and indium phosphide. These alloys are used in the manufacture of electronic devices such as microprocessors and memory chips which are widely used in an increasing range of modern electronic products. With the increasing miniaturization of these devices more stringent demands are placed on the quality of the materials produced by this process. In particular spatial variations in the composition of the alloy or defects in the atomic lattice can severely impair the performance of the end product. It is known that the planar, solid/liquid interface of a steadily freezing binary alloy may become unstable to a cellular structure (Rutter & Chalmers 1953; Morris & Winegard 1969; McCartney & Hunt 1981), resulting in unwanted compositional inhomogeneities in the solidified material. This is known as the morphological instability. The current technological importance of microchip technology has motivated increasing theoretical investigation of the morphological instability, and is the subject of a review by Coriell, McFadden & Sekerka (1985).

The first explanation of the morphological instability was given by Tiller *et al.* (1953) in terms of the mechanism of constitutional supercooling, the idea behind which is that the segregation of one component of the alloy (henceforth referred to as the solute) at the freezing solid/liquid interface gives rise to a solute boundary layer in the liquid adjacent to the interface. Since the freezing temperature of the alloy depends on its composition, under certain conditions the liquid in the solute

boundary layer may be beneath its freezing temperature and thus supercooled. In such a situation perturbations of the interface will encounter supercooled fluid and therefore may be expected to grow, rendering the interface unstable. From these considerations Tiller *et al.* (1953) deduced the constitutional supercooling criterion $G/mG_c > 1$ for stability, where G and G_c are respectively the temperature and solute concentration gradients measured at the interface, and m is the slope of the liquidus line on the equilibrium phase diagram of the alloy. The linear stability analysis for this situation was first conducted by Mullins & Sekerka (1964). This has been extended to the weakly nonlinear regime by Wollkind & Segel (1970) and Wollkind, Oulton & Sriranganathan (1984).

Fluid motion within the melt is known to have considerable influence on the stability of the system and has been the subject of reviews by Coriell & Sekerka (1981) and Glicksman, Coriell & McFadden (1986). The effect of model forced flows, representing larger scale fluid motions in the melt, on the morphological stability of the solid/liquid interface has been considered analytically by Delves (1968, 1971) for Blasius and quadratic flow profiles, and numerically by Coriell *et al.* (1984) for a Couette flow. In both cases a linear stability analysis was employed which predicted some stabilization of the morphological instability for disturbances with wave vectors in the direction of fluid flow. Brattkus & Davis (1988*a*) conducted a weakly nonlinear analysis for a model flow representing the solidification of a rotating disk. They found that the flow over the interface induced by rotation promotes a long-wave instability. Brattkus & Davis (1988*b*) and McFadden, Coriell & Alexander (1988) have considered the effect of a planar stagnation-point flow. In particular Brattkus & Davis (1988*b*) found a destabilization of the system for long-wavelength disturbances which propagate against the direction of the flow. McFadden *et al.* (1988) conducted a numerical investigation of this situation and predicted the flow to have a stabilizing effect on the morphological stability of the system.

McFadden *et al.* (1984) and Fang *et al.* (1985) considered theoretically and experimentally the stability of a system in which a long, vertical, heated wire is surrounded by a cylindrical melt confined by an annulus of its solid. The simplest case of a single-component melt was considered and a convective instability was observed for a temperature difference between wire and solid approximately one tenth that required for a rigid (non-freezing) interface. These results indicate the possibility of strong coupling between flow and morphological modes of instability.

In this paper we investigate the interaction of the morphological mode of instability of a planar interface with the hydrodynamic, shear mode of instability due to the presence of a model boundary-layer flow adjacent to the interface. The velocity profile we adopt is the asymptotic suction profile. This has the advantage that it is an exact solution of the Navier–Stokes equations and so we avoid making the boundary-layer approximation as was done by Delves (1968, 1971). Further we are able to examine the linear stability of the boundary layer in this situation, a possibility precluded by the choice of the absolutely linearly stable Couette flow considered by Coriell *et al.* (1984).

The stability of the asymptotic suction profile over a rigid interface has received much attention over the years. It has been reviewed and extended by both Chiarulli & Freeman (1948) and Hughes & Reid (1965). These authors obtained an Orr–Sommerfeld equation from a linear stability analysis that governed the onset of instability. They developed approximations in the limit of large Reynolds number to the solutions of the Orr–Sommerfeld equation by heuristic arguments. Subsequently

Lakin & Reid (1982) derived uniformly valid approximations to the Orr–Sommerfeld equation in this limit and so determined more accurate values for the critical Reynolds number. Numerical solutions of the Orr–Sommerfeld equation have been obtained by Ng & Reid (1980) and Mack (quoted in Drazin & Reid 1981). Hocking (1975) has conducted a weakly nonlinear analysis.

In §2 we present a mathematical model and demonstrate the existence of two length and velocity scales, one associated with the solute field and hence the morphological instability, and the other associated with the shear flow instability. In §3 we conduct a linear stability analysis to obtain an equation for the perturbed solute concentration coupled to an Orr–Sommerfeld equation for the perturbed flow. In §4 an asymptotic solution of these equations is presented for the morphological mode of instability in the realistic limit of the Schmidt number tending to infinity. The linearized equations are solved numerically in §5 and results presented for values of the Reynolds number for which the analysis of §4 is not valid. In §6 we rescale the equations onto the scales appropriate to the shear flow instability and prove a form of Squire's theorem, allowing us to consider only two-dimensional disturbances. A heuristic, asymptotic analysis of the limit Reynolds number tending to infinity is then presented in §7 based on the approach of Hughes & Reid (1965).

We show that the effect of the shear flow on the morphological stability is greatest for disturbances with wave vectors aligned with the flow. Such disturbances may stabilize or destabilize the morphological mode and we show, from the analysis in §4, that this is characterized by just two parameters: the segregation coefficient and the wavenumber of the disturbance. The analysis given in this section also provides an analytical description of the numerical calculations of Coriell *et al.* (1984) for low shear. From the numerical calculations for the lead–tin alloy considered in §5 we find that the effect of increasing the Reynolds number is to further stabilize the morphological mode as well as to narrow the range of unstable wavenumbers at the onset of instability. From the asymptotic and numerical calculations in §§6 and 7 we find that the large Schmidt numbers associated with real alloys imply that the presence of the interface has negligible effect on the hydrodynamic stability of the boundary layer. However for lower values of the Schmidt number the effect is more pronounced, leading to a stabilization.

2. The governing equations

We consider a dilute binary alloy freezing at a solid/liquid interface due to the presence of an imposed temperature gradient. The liquid phase is in motion with a non-zero component of velocity parallel to the solid/liquid interface. The alloy is composed of two species, the more dilute of which we shall refer to as the solute. In particular, we assume that the interface is initially planar and advances into the fluid with an average speed V_0^*. We locate our coordinate system in a frame of reference coincident with the average position of the interface, which is given by $z^* = 0$. The fluid is assumed to be of semi-infinite extent and to occupy the region $z^* > 0$. The free-stream velocity and solute concentrations are prescribed in the liquid phase far from the interface and can be considered to represent the behaviour of larger scale transport processes in a real crystal-growth melt. The configuration of the system is shown in figure 1. Further we adopt the following assumptions:

(i) We neglect the effect of gravity.

(ii) There is no change of density of the alloy on solidification.

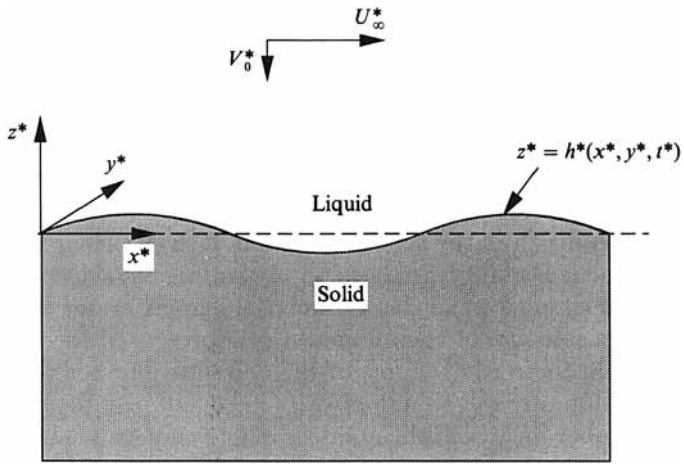

FIGURE 1. The configuration diagram.

(iii) The thermal properties of the solid and the liquid phase are equal and thermal diffusivities are much greater than the solute diffusivity in the liquid phase.
(iv) Latent heat production at the interface is negligible.
(v) The liquid is incompressible.
(vi) The effect of diffusion in the solid phase is negligible.
(vii) The alloy is dilute.

Although buoyancy effects are known to be important in real crystal growth systems (Glicksman *et al.* 1986) we are concerned here with the interaction of the morphological instability of the interface with the hydrodynamic instability of the fluid flow and hence neglect them by adopting assumption (i). Assumptions (ii), (iii) and (iv), although not strictly true for most alloys, can be shown to have no qualitative effect on the morphological instability (Mullins & Sekerka 1964) and have the advantage that they permit the temperature to be decoupled from the solute and fluid velocity fields. Hence we take the temperature to be of the fixed form:

$$T^* = T^*_i + G^* z^*, \tag{2.1}$$

where T^* is the temperature, T^*_i is the temperature at the planar interface and G^* is the imposed temperature gradient. For most semiconducting alloys the diffusion coefficient of solute in the solid is several orders of magnitude smaller than that of the liquid phase, hence our assumption (vi).

Under these assumptions the Navier–Stokes equations and convection–diffusion equation govern the transport of momentum and solute respectively. Hence

$$\frac{\partial \boldsymbol{u}^*}{\partial t^*} + \boldsymbol{u}^* \cdot \boldsymbol{\nabla} \boldsymbol{u}^* = -\frac{1}{\rho} \boldsymbol{\nabla} p^* + \nu \nabla^2 \boldsymbol{u}^*, \tag{2.2}$$

$$\frac{\partial C^*}{\partial t^*} + \boldsymbol{u}^* \cdot \boldsymbol{\nabla} C^* = \tilde{D} \nabla^2 C^*, \tag{2.3}$$

and we further assume the liquid phase is incompressible and so

$$\boldsymbol{\nabla} \cdot \boldsymbol{u}^* = 0, \tag{2.4}$$

where $\boldsymbol{u}^*$, p^*, C^* are the dimensional velocity, pressure and solute concentration respectively, ν and ρ are the kinematic viscosity and density of the fluid and $\tilde{D}$ is the solute diffusion coefficient in the liquid phase.

The boundary conditions at the solid/liquid interface, which we describe by $z^* = h^*(x^*, y^*, t^*)$, are

$$(\boldsymbol{u}^* + V_0^* \hat{\boldsymbol{z}}) \cdot \hat{\boldsymbol{n}} = 0, \tag{2.5}$$

$$(\boldsymbol{u}^* + V_0^* \hat{\boldsymbol{z}}) \times \hat{\boldsymbol{n}} = 0, \tag{2.6}$$

$$\tilde{D} \nabla C^* \cdot \hat{\boldsymbol{n}} = (k-1)\, C^* (V_0^* \hat{\boldsymbol{z}} + V_b^*) \cdot \hat{\boldsymbol{n}}, \tag{2.7}$$

$$T^* = T_0^* + mC^* + T_0^* \mathscr{U}^* \mathscr{K}^*. \tag{2.8}$$

Equation (2.5) follows from conservation of mass at the interface, where $\hat{\boldsymbol{n}}$ is the unit normal to the interface directed towards the fluid. Equation (2.6) is the no-slip condition. Equation (2.7) expresses the conservation of solute across the interface, where k is known as the segregation or partition coefficient and V_b^* is the velocity of the solid/liquid interface in our moving frame of reference. The last boundary condition (2.8) describes the dependence of the freezing temperature of a binary alloy upon its composition and also, in its last term, includes capillarity effects sometimes referred to as the Gibbs–Thompson effect. Here T_0^* is the freezing temperature of the pure substance, m the liquidus slope, $\mathscr{U}^*$ is the capillarity constant and $\mathscr{K}^*$ is the curvature of the interface (assumed to be negative for a convex projection into the fluid). In general the freezing temperature of an alloy is a complicated function of its concentration; however, the alloy is dilute and so (2.8) assumes a linear form of this function.

The far-field boundary conditions are

$$\boldsymbol{u}^* \to (U_\infty^*, 0, -V_0^*), \tag{2.9}$$

$$C^* \to C_\infty^*, \tag{2.10}$$

as $z^* \to \infty$.

We consider the steady state corresponding to a planar interface, with a velocity field of the form

$$\boldsymbol{u}_0^*(\boldsymbol{x}^*) = (U_0^*(z^*), 0, -V_0^*), \tag{2.11}$$

and a concentration profile $C_0^*(z^*)$ dependent only on the z^* coordinate. Then a steady-state solution to (2.2)–(2.4) with boundary conditions (2.5)–(2.10) is

$$U_0^*(z^*) = U_\infty^* \left(1 - \exp\left(\frac{-V_0^* z^*}{\nu}\right)\right), \tag{2.12}$$

$$C_0^*(z^*) = C_\infty^* \left(1 + \frac{1-k}{k} \exp\left(\frac{-V_0^* z^*}{\tilde{D}}\right)\right), \tag{2.13}$$

$$p_0^*(\boldsymbol{x}^*) = p_0^*, \tag{2.14}$$

and then (2.1) yields

$$T^*(z^*) = T_0^* + mC_0^*(0) + G^* z^*. \tag{2.15}$$

The velocity profile is well known and is called the asymptotic suction profile. From (2.12) and (2.13) we observe that there are two distinct sets of velocity and length scales associated with this problem. The first set, $V_s = U_\infty^*$ and $L_s = \nu / V_0^*$ is associated with the velocity profile and will be referred to as the shear-flow scalings. The second set, $V_c = V_0^*$ and $L_c = \tilde{D}/V_0^*$ are the solute-field scalings.

Initially, we shall adopt the solute-field scalings and non-dimensionalize the problem by putting

$$\left.\begin{aligned} &\boldsymbol{x}^* = L_c\boldsymbol{x}, \quad \boldsymbol{u}^* = V_c\boldsymbol{u}, \quad t^* = (L_c/V_c)\,t, \quad p^* = \rho V_c^2 p, \\ &T^* = T_0^* T, \quad C^* = C_\infty^* C, \quad h^* = L_c h\left(\frac{x^*}{L_c}, \frac{y^*}{L_c}, \frac{t^* V_c}{L_c}\right), \quad G^* = T_0^* G/L_c, \end{aligned}\right\} \tag{2.16}$$

in which case the following non-dimensional, governing equations are obtained:

$$\frac{\partial \boldsymbol{u}}{\partial t} + \boldsymbol{u}\cdot\nabla\boldsymbol{u} = -\nabla p + Sc\,\nabla^2\boldsymbol{u}, \tag{2.17}$$

$$\frac{\partial C}{\partial t} + \boldsymbol{u}\cdot\nabla C = \nabla^2 C, \tag{2.18}$$

$$\nabla\cdot\boldsymbol{u} = 0, \tag{2.19}$$

where $Sc = \nu/\tilde{D}$, is the Schmidt number.

The boundary conditions imposed on the crystal melt interface $z = h(x, y, t)$ are

$$(\hat{\boldsymbol{z}} + \boldsymbol{u})\cdot\hat{\boldsymbol{n}} = 0, \tag{2.20}$$

$$(\hat{\boldsymbol{z}} + \boldsymbol{u})\times\hat{\boldsymbol{n}} = 0, \tag{2.21}$$

$$\nabla C\cdot\hat{\boldsymbol{n}} = (k-1)\,C(\hat{\boldsymbol{z}} + \boldsymbol{V}_b)\cdot\hat{\boldsymbol{n}}, \tag{2.22}$$

$$T = 1 + MC + \hat{\mathscr{U}}\mathscr{K}, \tag{2.23}$$

where $M = mC_\infty^*/T_0^*$ is the non-dimensional liquidus slope, $\hat{\mathscr{U}} = \mathscr{U}^* V_0/\tilde{D}$ is the non-dimensional capillarity and $\mathscr{K}$ is the non-dimensional curvature of the interface.

We define a Reynolds number Re by

$$Re = U_\infty^*/V_0^*, \tag{2.24}$$

so the far-field boundary conditions are

$$\boldsymbol{u} \to (Re, 0, -1), \quad C \to 1 \quad \text{as} \quad z \to \infty. \tag{2.25}$$

The steady-state solutions (2.11)–(2.14) then become

$$\boldsymbol{u}_0(\boldsymbol{x}) = (U_0(z), 0, -1), \tag{2.26}$$

where

$$U_0(z) = Re\,(1 - \exp(-z/Sc)), \tag{2.27}$$

and

$$C_0(z) = 1 - \hat{G}_c \exp(-z), \tag{2.28}$$

$$p_0(\boldsymbol{x}) = p_0, \tag{2.29}$$

$$T(z) = 1 + MC_0(0) + Gz, \tag{2.30}$$

where $\hat{G}_c$ is the non-dimensional concentration gradient at the interface given by

$$\hat{G}_c = C_0'(0) = (k-1)/k. \tag{2.31}$$

3. Linear stability analysis

We next examine the stability of the steady-state solutions using linear perturbation theory. We proceed in the standard way and put

$$\boldsymbol{u}(\boldsymbol{x}) = (U_0(z) + \tilde{u}(\boldsymbol{x}), \tilde{v}(\boldsymbol{x}), -1 + \tilde{w}(\boldsymbol{x})), \tag{3.1}$$

$$C(\boldsymbol{x}) = C_0(z) + \tilde{c}(\boldsymbol{x}), \tag{3.2}$$

$$p(\boldsymbol{x}) = p_0 + \tilde{p}(\boldsymbol{x}), \tag{3.3}$$

$$h = \tilde{h}(x, y, t), \tag{3.4}$$

where
$$(\tilde{u}, \tilde{v}, \tilde{w}, \tilde{c}, \tilde{p})(\boldsymbol{x}, t) = (\bar{u}, \bar{v}, \bar{w}, \bar{C}, \bar{p})(z) \exp(\mathrm{i}\hat{\alpha}(x - \hat{c}t) + \mathrm{i}\hat{\beta}y), \tag{3.5}$$

$$\tilde{h}(x, y, t) = \delta \exp(\mathrm{i}\hat{\alpha}(x - \hat{c}t) + \mathrm{i}\hat{\beta}y), \tag{3.6}$$

$\hat{\alpha}$ and $\hat{\beta}$ are the wavenumbers in the x- and y-directions respectively and $\hat{c}$ is the wave speed.

We now linearize the governing equations (2.17)–(2.19) to obtain

$$[Sc(\mathrm{D}^2 - \hat{\gamma}^2) + \mathrm{D} + \mathrm{i}\hat{\alpha}(\hat{c} - U_0(z))]\,\bar{u}(z) = \bar{w}(z)\,U_0'(z) + \mathrm{i}\hat{\alpha}\bar{p}(z), \tag{3.7}$$

$$[Sc(\mathrm{D}^2 - \hat{\gamma}^2) + \mathrm{D} + \mathrm{i}\hat{\alpha}(\hat{c} - U_0(z))]\,\bar{v}(z) = \mathrm{i}\hat{\beta}\bar{p}(z), \tag{3.8}$$

$$[Sc(\mathrm{D}^2 - \hat{\gamma}^2) + \mathrm{D} + \mathrm{i}\hat{\alpha}(\hat{c} - U_0(z))]\,\bar{w}(z) = \mathrm{D}\bar{p}(z), \tag{3.9}$$

$$\mathrm{i}\hat{\alpha}\bar{u}(z) + \mathrm{i}\hat{\beta}\bar{v}(z) + \mathrm{D}\bar{w}(z) = 0, \tag{3.10}$$

$$[\mathrm{D}^2 - \hat{\gamma}^2 + \mathrm{D} + \mathrm{i}\hat{\alpha}(\hat{c} - U_0(z))]\,\bar{C}(z) = \bar{w}(z)\,C_0'(z), \tag{3.11}$$

where D is the differential operator d/dz and $\hat{\gamma}^2 = \hat{\alpha}^2 + \hat{\beta}^2$. Using (3.10) to eliminate perturbed pressure $\bar{p}(z)$ yields

$$[Sc(\mathrm{D}^2 - \hat{\gamma}^2)^2 + \{\mathrm{D} + \mathrm{i}\hat{\alpha}(\hat{c} - U_0(z))\}(\mathrm{D}^2 - \hat{\gamma}^2) + \mathrm{i}\hat{\alpha}U_0''(z)]\,\bar{w}(z) = 0, \tag{3.12}$$

which, together with the differential equation for the perturbed solute concentration (3.11), are our working linearized equations for $\bar{w}(z)$ and $\bar{C}(z)$.

The boundary conditions at the perturbed interface (2.20) and (2.21) may be transferred to $z = 0$ yielding

$$\bar{w}(0) = 0, \tag{3.13}$$

$$\bar{u}(0) = -U_0'(0)\,\delta, \tag{3.14}$$

$$\bar{v}(0) = 0. \tag{3.15}$$

Further (3.14) and (3.15) may be combined using (3.10) to give

$$\mathrm{D}\bar{w}(0) = \mathrm{i}\hat{\alpha}\,Re\,\delta/Sc, \tag{3.16}$$

and (2.22) and (2.23) yield

$$\delta\hat{G}_c(\mathrm{i}\hat{\alpha}\hat{c} - k) + \mathrm{D}\bar{C}(0) - (k-1)\,\bar{C}(0) = 0, \tag{3.17}$$

$$\frac{\bar{C}(0)}{\hat{G}_c} = \delta\left\{\frac{1}{Sk} - 1 + \frac{\hat{\mathscr{U}}\hat{\gamma}^2}{M\hat{G}_c}\right\}, \tag{3.18}$$

where Sk is the Sekerka number defined by $Sk = M\hat{G}_c/G$.

The far-field boundary conditions are

$$\bar{w}(z), \mathrm{D}\bar{w}(z), \bar{C}(z) \to 0 \quad \text{as} \quad z \to \infty. \tag{3.19}$$

For given wavenumbers $\hat{\alpha}$ and $\hat{\beta}$, Reynolds number Re and Sekerka number Sk, as well as the parameters k, Sc, $\hat{\mathscr{U}}$ and M, the equations (3.11) and (3.12) together with boundary conditions (3.13) and (3.16)–(3.19) define an eigenvalue problem for $\hat{c}$. Let $\hat{c}_i$ denote the imaginary part of $\hat{c}$; then the system is linearly stable if $\hat{\alpha}\hat{c}_i$ is negative for all wavenumbers, otherwise it is unstable.

If either the wavenumber $\hat{\alpha}$ or Reynolds number Re are zero (or both) then, as Delves (1971) noted in a similar situation, the neutral curve is given by

$$\frac{1}{Sk}-1+\frac{\hat{\mathscr{U}}\hat{\gamma}^2}{M\hat{G}_c}=\frac{-k}{k-\frac{1}{2}+R(\hat{\gamma})} \tag{3.20}$$

where $R(\hat{\gamma})=(\frac{1}{4}+\hat{\gamma}^2)^{\frac{1}{2}}$.

This is the result of Mullins & Sekerka (1964) for the morphological instability in the absence of fluid flow under the assumptions of our model. The case of $\hat{\alpha}=0$ corresponds to modes perpendicular to the flow direction and so these modes are unaffected by the shear flow redistributing the solute. When the Reynolds number is zero there is no imposed flow and hence we expect to recover the Mullins & Sekerka result.

4. An asymptotic solution for large Schmidt number

In real alloy systems the Schmidt number is large, typically between 10 and 100; so in order to make a first step to determine the effect of the shear flow on the morphological stability of the system we consider the solution of (3.11) and (3.12) with boundary conditions (3.13) and (3.16)–(3.19) in the limit $Sc\to\infty$ with Re order one and fixed. So we put

$$\bar{w}(z)=\bar{w}_0(z)+\frac{\bar{w}_1(z)}{Sc}+\frac{\bar{w}_2(z)}{Sc^2}+O(Sc^{-3}), \tag{4.1}$$

$$\bar{C}(z)=\bar{C}_0(z)+\frac{\bar{C}_1(z)}{Sc}+\frac{\bar{C}_2(z)}{Sc^2}+O(Sc^{-3}), \tag{4.2}$$

$$\hat{c}=\hat{c}_0+\frac{\hat{c}_1}{Sc}+\frac{\hat{c}_2}{Sc^2}+O(Sc^{-3}), \tag{4.3}$$

$$S=S_0+\frac{S_1}{Sc}+\frac{S_2}{Sc^2}+O(Sc^{-3}), \tag{4.4}$$

as $Sc\to\infty$, where $S=1/Sk$ is the inverse Sekerka number. The governing equations (3.11) and (3.12) are then successively solved at each order of the small parameter $1/Sc$.

4.1. *Leading order*

The leading-order terms of the governing equations and boundary conditions give a simple pair of ordinary differential equations which are easily solved explicitly to give

$$S_0-1+\frac{\hat{\mathscr{U}}\hat{\gamma}^2}{M\hat{G}_c}=\frac{\mathrm{i}\hat{\alpha}\hat{c}_0-k}{k-\frac{1}{2}+R}, \tag{4.5}$$

where

$$R=(\hat{\gamma}^2+\tfrac{1}{4}-\mathrm{i}\hat{\alpha}\hat{c}_0)^{\frac{1}{2}}. \tag{4.6}$$

This is the leading-order approximation to the dispersion relation. Upon considering the imaginary part of (4.5) the exchange of stabilities for this approximate dispersion relation can be shown to hold, that is setting $\mathrm{Im}\,(\hat{\alpha}\hat{c}_0)$ to zero implies that $\mathrm{Re}\,(\hat{\alpha}\hat{c}_0)$ is equal to zero. Thus on the curve of marginal stability we put $\hat{\alpha}\hat{c}_0=0$ to obtain

$$S_0-1+\frac{\hat{\mathscr{U}}\hat{\gamma}^2}{M\hat{G}_c}=\frac{-k}{k-\frac{1}{2}+R}, \tag{4.7}$$

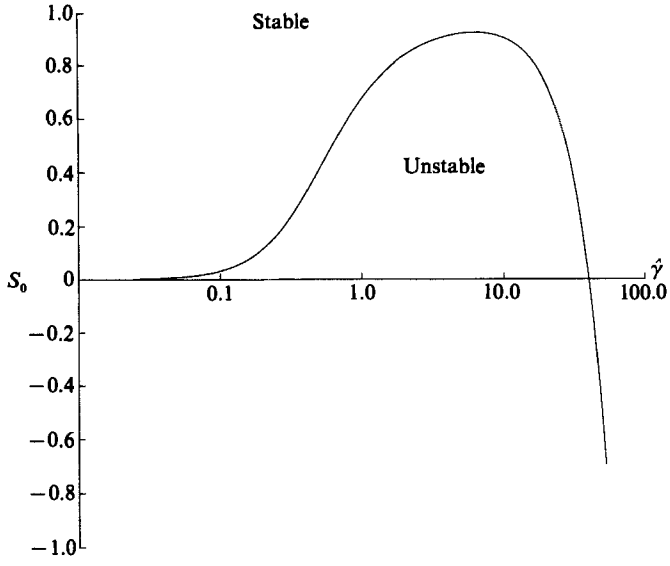

FIGURE 2. The leading-order approximation S_0 to the inverse Sekerka number on the curve of marginal stability, as given by (4.7), for a range of wavenumbers $\hat{\gamma}$. The material parameters used are those of table 1 for the model lead/tin alloy with a far-field concentration of 0.01 wt % and a growth speed of 10^{-4} cm/s.

Kinematic viscosity	ν	2.43×10^{-3}	cm^2/s
Solute diffusion coefficient	$\tilde{D}$	3.0×10^{-5}	cm^2/s
Schmidt number	Sc	81	
Liquidus slope	m	−2.33	K/wt %
Capillarity parameter	$\mathscr{U}^*$	1.665×10^{-8}	cm
Partition coefficient	k	0.3	
Melting point of lead	T_0^*	600.6	K

TABLE 1. Values of physical parameters for model lead–tin alloy

where $$R = (\hat{\gamma}^2 + \tfrac{1}{4})^{\frac{1}{2}}. \tag{4.8}$$

This is the equivalent result of Mullins & Sekerka (1964) for the morphological instability in the absence of flow in the melt. Thus at leading order the flow has had no effect on the redistribution of solute controlling the morphological instability. Comparing (2.27) and (2.28) we can see that for large Schmidt number the solute boundary layer is 'embedded' in the viscous boundary layer and hence that the velocity profile is not 'seen' by the freezing interface. A typical leading-order marginal curve, i.e. a plot of the curve described by (4.7), is shown in figure 2 for a model lead/tin alloy. The appropriate material parameters are given in table 1.

4.2. *First order*

We now seek a first-order correction to the leading-order marginal state. We set $\hat{c}_0$ to zero in the leading-order solution, solve the first-order problem and after some algebra arrive at the following dispersion relation

$$S_1 = \mathrm{i}\hat{\alpha}\{\hat{c}_1 L(k, \hat{\gamma}) - Re\, U(k, \hat{\gamma})\}, \tag{4.9}$$

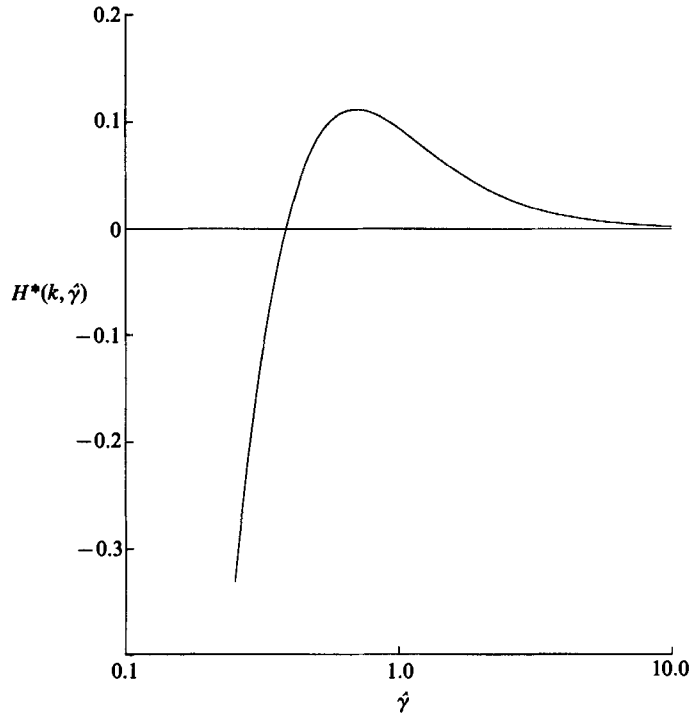

FIGURE 3. The function $H^*(k,\hat{\gamma})$ for a partition coefficient $k = 0.3$, corresponding to the model lead/tin alloy of table 1, plotted against wavenumber $\hat{\gamma}$.

where
$$U(k,\hat{\gamma}) = \frac{1}{k-\frac{1}{2}+R}\left\{\frac{(k+\hat{\gamma})(2\hat{\gamma}+1)}{\hat{\gamma}^2} - \frac{1}{\hat{\gamma}} - \frac{k}{4(k-\frac{1}{2}+R)R^2}\right\} - \frac{2\hat{\gamma}+1}{\hat{\gamma}^2}, \tag{4.10}$$

and
$$L(k,\hat{\gamma}) = \frac{1}{k-\frac{1}{2}+R}\left\{1 - \frac{k}{2R(k-\frac{1}{2}+R)}\right\}. \tag{4.11}$$

On the marginal curve $\hat{c}_1$ is real, as are S_1, $\hat{\alpha}$, Re, $L(k,\hat{\gamma})$ and $U(k,\hat{\gamma})$; hence to satisfy (4.9) S_1 must be taken as zero. Thus there is no contribution to the inverse Sekerka number at this order. However the wave speed of the disturbance is given by

$$\hat{c}_1 = Re\, H^*(k,\hat{\gamma}), \tag{4.12}$$

where
$$H^*(k,\hat{\gamma}) = U(k,\hat{\gamma})/L(k,\hat{\gamma}). \tag{4.13}$$

The function $H^*(k,\hat{\gamma})$ for the case of a lead/tin alloy is shown in figure 3. In figure 4 we indicate in $(\hat{\gamma},k)$-space the parameter regime for $\hat{c}_1$ to be positive or negative, corresponding to forward- and backward-travelling waves respectively. The observed wave speed at the critical wavenumber is generally positive unless the growth speed of the crystal is sufficiently fast corresponding to a large value of the capillarity parameter $\hat{\mathscr{U}}$. For any particular wavenumber it is seen, from the above analysis, that the sign of the wave speed is dependent solely on the partition coefficient k (for order-one Reynolds number), although it should be noted that the asymptotic result will only hold for $\hat{\gamma}^2 > 1/Sc$ otherwise a different balance of terms is required in the asymptotic analysis. We also note that the speed of the disturbance is proportional to the Reynolds number and hence to the speed of the fluid far in the bulk of the melt.

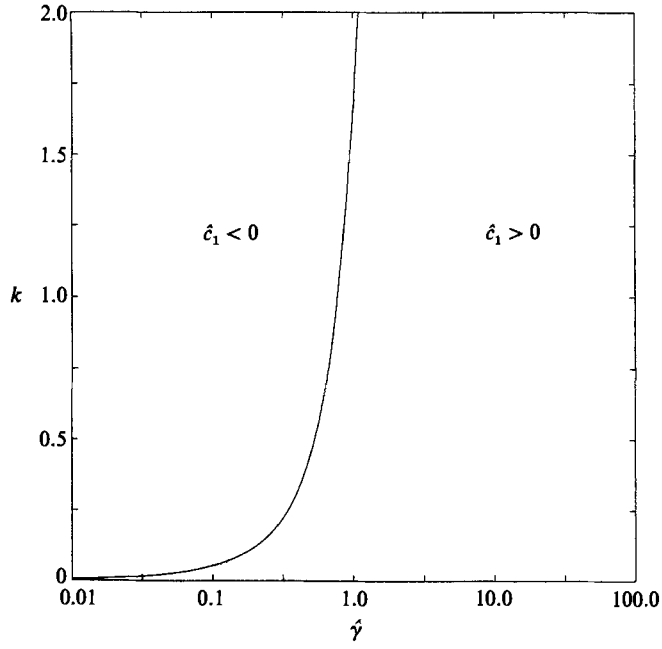

FIGURE 4. The sign of the wave speed $\hat{c}_1$ as a function of the partition coefficient k and wavenumber $\hat{\gamma}$ on the curve of marginal stability.

4.3. *Second order*

We take $\hat{c}_1$ real as given by (4.12), solve the governing equations at this level of approximation and take the real and imaginary parts of the resulting dispersion relation to obtain the following expression for the growth rate of the disturbance:

$$\hat{\alpha}\,\mathrm{Im}\,(\hat{c}_2) = (k-\tfrac{1}{2}+R)\left\{\hat{\alpha}^2 Re^2\left\{f_1-\left[\frac{(k+\hat{\gamma})f_1-d_1-f_2}{k-\tfrac{1}{2}+R}\right]\right\}-S_2\right\}, \tag{4.14}$$

where $f_1 = f_1(\hat{\gamma}, k), f_2 = f_2(\hat{\gamma}, k)$ and $d_1 = d_1(\hat{\gamma}, k)$ are independent of $\hat{\alpha}$ and given in the Appendix. For stability we require $\hat{\alpha}\,\mathrm{Im}\,(\hat{c}_2)$ negative, and since $(k-\frac{1}{2}+R)$ is positive for all $k\,(>0)$ and $\hat{\gamma}$ then the stability criterion at this order is

$$S_2 \geqslant \hat{\alpha}^2 Re^2\left\{f_1-\left[\frac{(k+\hat{\gamma})f_1-d_1-f_2}{k-\tfrac{1}{2}+R}\right]\right\}. \tag{4.15}$$

Clearly $\hat{\alpha}$ or Re equal to zero results in no correction to S as discussed at the end of §3. As f_1, f_2 and d_1 are all independent of $\hat{\alpha}$, $|S_2|$ will be maximum when $\hat{\alpha} \equiv \hat{\gamma}$, i.e. for modes parallel to the flow direction, in which case the criterion for marginal stability gives that $\hat{\alpha}\,\mathrm{Im}\,(\hat{c}_2) = 0$ and so we obtain from (4.15) that

$$\frac{S_2}{Re^2} = \hat{\alpha}^2\left\{f_1-\left[\frac{(k+\hat{\alpha})f_1-d_1-f_2}{k-\tfrac{1}{2}+R}\right]\right\}. \tag{4.16}$$

The quantity S_2/Re^2 is plotted for the case $k = 0.3$ in figure 5. Over a wide range of wavenumbers it is negative, corresponding to a stabilization of modes parallel to the flow. Hence the modes perpendicular to the flow will be the most unstable, i.e. they become unstable at a lower Sekerka number than any other modes. In figure 6

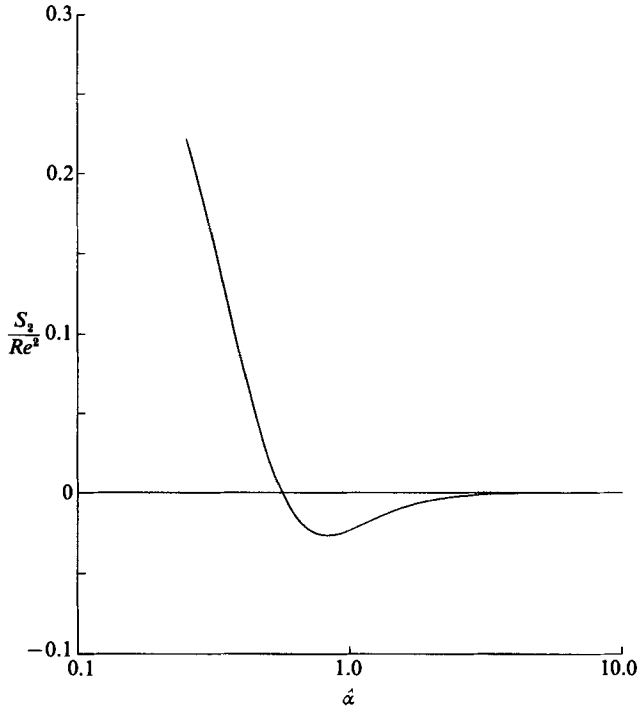

FIGURE 5. The correction S_2 to the inverse Sekerka number given by (4.16) at marginal stability plotted against wavenumber for disturbances with wave vectors in the x-direction. The partition coefficient is 0.3.

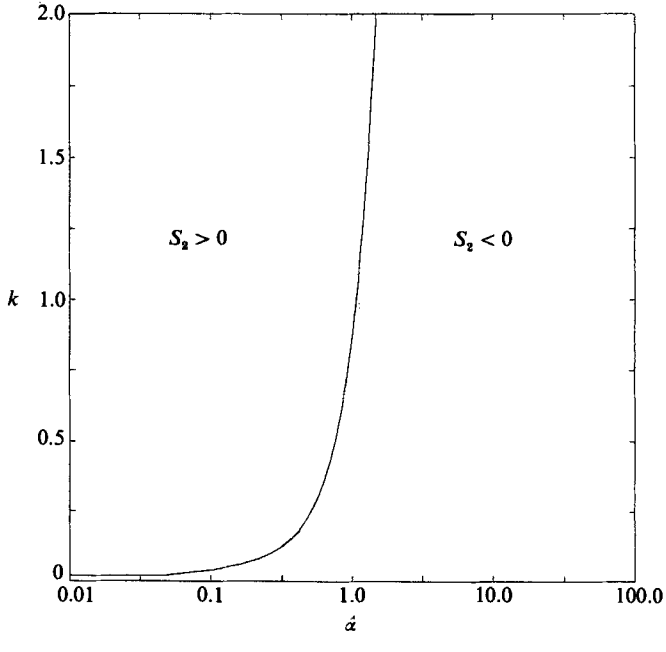

FIGURE 6. The sign of the second-order correction S_2 to the inverse Sekerka number at marginal stability as a function of wavenumber $\hat{\alpha}$ and partition coefficient k.

we indicate the sign of S_2/Re^2 in $(\hat{\alpha}, k)$-space. At the high wavenumbers typical of the onset of morphological instability the quantity S_2/Re^2 is negative, in which case modes perpendicular to the flow will be the most unstable.

The analysis above can be extended to more general boundary-layer profiles because the expressions for $\hat{c}_1$ and S_2 only require $U_0'(0)$ to account for the flow. Related to this is the observation that on the scale of the solute boundary layer the horizontal component of the flow is

$$U_0(z) = \frac{Re}{Sc} z + O(Sc^{-2}) \quad \text{as} \quad Sc \to \infty,$$

and so is approximately a plane Couette flow. The effect of such a flow on the morphological stability has been considered by Coriell *et al.* (1984) who conducted a linear stability analysis and solved the resulting eigenvalue problem numerically. We have compared the analytic expressions for S_0, S_2 and $\hat{c}_1$ with their numerical results and obtained good agreement, for low values of their shear parameter. Greater values of this parameter correspond to large values of our Reynolds number for which the analysis presented above is not valid.

5. The numerical solution of the linearized equations

In order to solve numerically the eigenvalue problem posed by the differential equations (3.11) and (3.12) and associated boundary conditions (3.13), (3.16)–(3.19) for the Sekerka number Sk at a given wavenumber and Reynolds number we adopted the following procedure. This sixth-order system was re-expressed as a set of twelve first-order differential equations for the real and imaginary parts of $\bar{w}(z)$, $\bar{C}(z)$ and their derivatives. The far-field boundary conditions (3.19) were not employed directly but were replaced by an equivalent set of six boundary conditions at a finite value of z. This equivalent set was derived from asymptotic forms of the solutions of (3.11) and (3.12) for large z and is an extension of the results given by Ng & Reid (1980) to include the solute field.

The interface deflection δ was eliminated from the interfacial boundary conditions (3.13), (3.16) and (3.17) using (3.18) to give six boundary conditions at $z = 0$. We require a further condition to fix the magnitude of the eigensolution (Keller 1976) which we chose to be $\bar{C}(0) = 1$. We set the imaginary part of c to zero and chose an initial guess for the Sekerka number Sk and the real part of c. We solved the system using the SUPORT code (Scott & Watts 1975) ignoring the solute flux boundary condition (3.17). We then iterated Sk and the real part of c employing the NAG nonlinear function solver subroutine C05NBF until (3.17) was satisfied, thus determining a point on the curve of marginal stability.

The marginal curves and the associated wave speeds for Schmidt numbers of 1 and 5 are shown in figures 7–10 for $\hat{\beta} = 0$ and various Reynolds numbers. Notice that the minima of the curves of marginal Sekerka number are rising monotonically with Reynolds number. For both Schmidt numbers the effect of the flow is to stabilize the morphological instability for modes parallel to the flow direction, the degree of stabilization increasing with Reynolds number. This is most pronounced for $Sc = 1$. For $Sc = 5$ the lower-wavenumber modes are the most stabilized which narrows the band of wavenumbers close to the critical Sekerka number. Thus modes perpendicular to the direction of flow remain the most unstable. Similar behaviour was found by McFadden *et al.* (1988) for the modes perpendicular to a planar stagnation-point flow. We also observe that for $Sc = 1$ the wave speed of the low

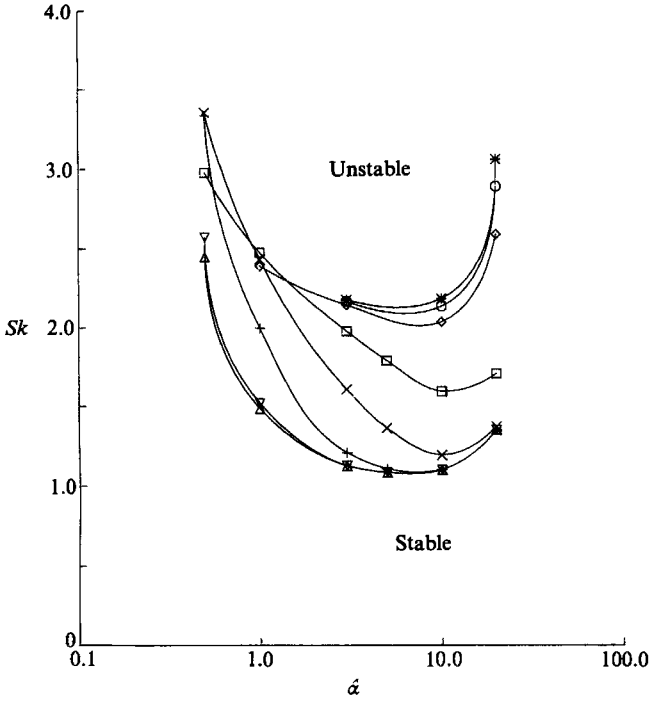

FIGURE 7. The Sekerka number Sk at marginal stability as a function of wavenumber $\hat{\alpha}$ for various Reynolds numbers. The symbols $\triangle$, ∇, $+$, $\times$, $\square$, $\diamond$, $\bigcirc$, $*$ indicate Reynolds numbers of 0, 1, 10, 100, 1000, 10000, 20000, and 30000 respectively. The material parameters are those of table 1 for the model lead/tin alloy but with a Schmidt number $Sc = 1$. The far-field concentration is 0.01 wt % and the growth speed is 10^{-4} cm/s.

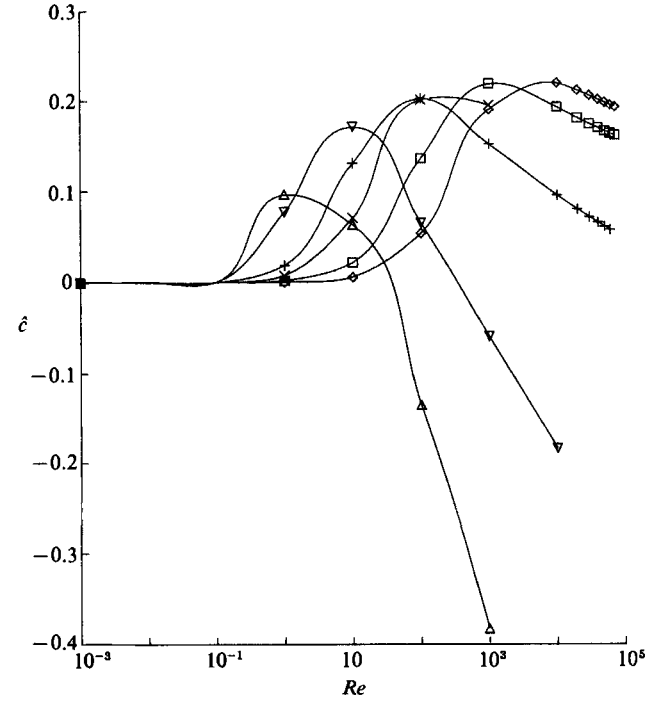

FIGURE 8. The dimensionless wave speed at marginal stability as a function of Reynolds number for various wavenumbers. The material and growth parameters are the same as in the case of figure 7. The symbols $\triangle$, ∇, $+$, $\times$, $\square$, $\diamond$ correspond to wavenumbers 0.5, 1, 3, 5, 10 and 20 respectively.

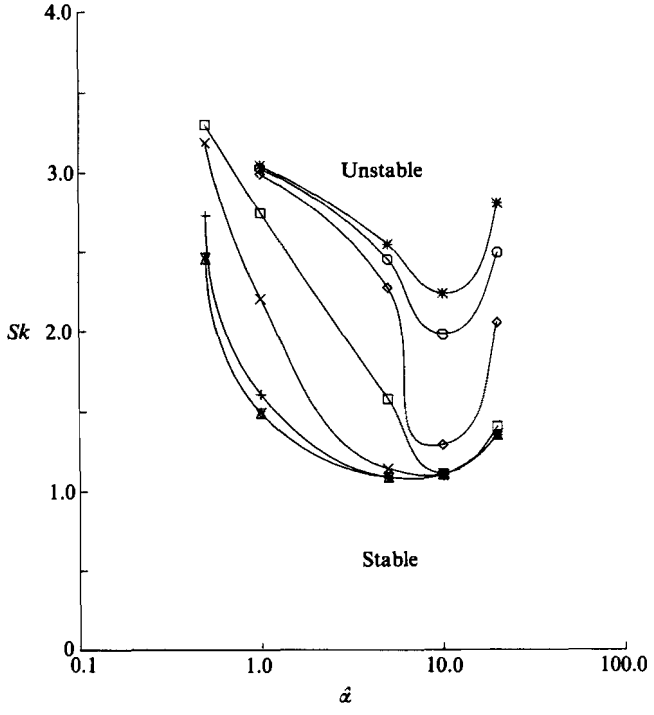

FIGURE 9. The Sekerka number Sk at marginal stability as a function of wavenumber $\hat{\alpha}$ for various Reynolds numbers. The symbols △, ▽, +, ×, □, ◇, ○, * indicate Reynolds numbers of 0, 1, 10, 100, 1000, 10000, 20000, and 30000 respectively. The material parameters are those of table 1 for the model lead/tin alloy but with a Schmidt number $Sc = 5$. The far-field concentration is 0.01 wt % and the growth speed is 10^{-4} cm/s.

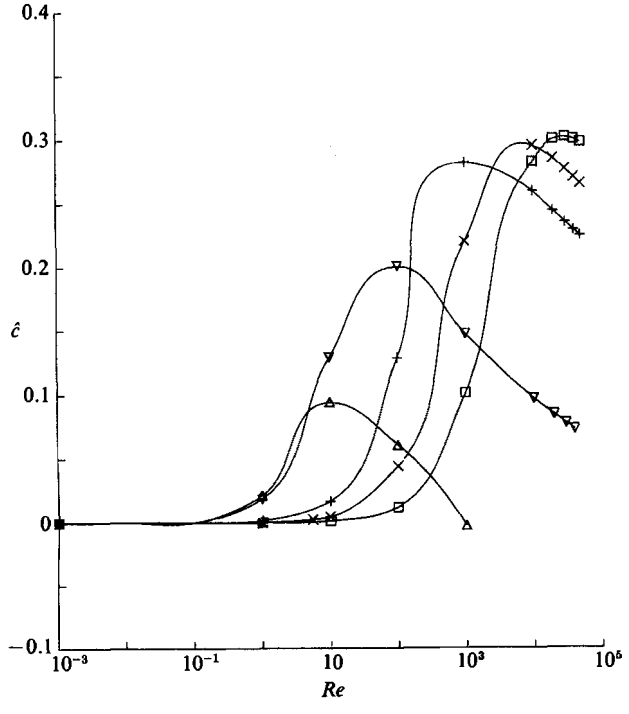

FIGURE 10. The dimensionless wave speed at marginal stability as a function of Reynolds number for various wavenumbers. The material and growth parameters are the same as in the case of figure 9. The symbols △, ▽, +, ×, □ correspond to wavenumbers 0.5, 1, 5, 10 and 20 respectively.

wavenumbers may become negative at a sufficiently large Reynolds number and from figure 10 we might expect a similar behaviour for the case $Sc = 5$. This corresponds to waves travelling in the opposite direction to the flow.

6. The hydrodynamic instability

We now rescale (3.7)–(3.11) onto the scalings appropriate to the shear flow as discussed in §2. We take a velocity scale $V_s = U_\infty^*$ and a length scale $L_s = \nu/V_0^*$ to give

$$[\mathrm{D}^2 + \mathrm{D} - \gamma^2 - \mathrm{i}\alpha Re\,(U_0 - c)]\,\bar{u}(z) = Re\,\bar{w}(z)\,U_0'(z) + \mathrm{i}\alpha Re\,\bar{p}(z), \tag{6.1}$$

$$[\mathrm{D}^2 + \mathrm{D} - \gamma^2 - \mathrm{i}\alpha Re\,(U_0 - c)]\,\bar{v}(z) = \mathrm{i}\beta Re\,\bar{p}(z), \tag{6.2}$$

$$[\mathrm{D}^2 + \mathrm{D} - \gamma^2 - \mathrm{i}\alpha Re\,(U_0 - c)]\,\bar{w}(z) = Re\,\mathrm{D}\,\bar{p}(z), \tag{6.3}$$

$$\mathrm{i}\alpha\bar{u}(z) + \mathrm{i}\beta\bar{v}(z) + \mathrm{D}\bar{w}(z) = 0, \tag{6.4}$$

$$[\mathrm{D}^2 + Sc\,\mathrm{D} - \gamma^2 - \mathrm{i}\alpha Re\,Sc\,(U_0 - c)]\,\bar{C}(z) = Re\,Sc\,C_0'(z)\,\bar{w}(z), \tag{6.5}$$

where $c = Re^{-1}\hat{c}$, $(\alpha, \beta, \gamma) = Sc\,(\hat{\alpha}, \hat{\beta}, \hat{\gamma})$ and from (2.12) and (2.13)

$$U_0(z) = 1 - \exp(-z), \tag{6.6}$$

$$C_0(z) = 1 + \frac{1-k}{k}\exp(-Sc\,z). \tag{6.7}$$

The boundary conditions (3.13)–(3.15), (3.17) and (3.18) become

$$\bar{u}(0) = -\delta, \tag{6.8}$$

$$\bar{v}(0) = 0, \tag{6.9}$$

$$\bar{w}(0) = 0, \tag{6.10}$$

$$\delta G_c\{\mathrm{i}\alpha c\,Re - k\,Sc\} + \mathrm{D}\bar{C}(0) - Sc\,(k-1)\,\bar{C}(0) = 0, \tag{6.11}$$

$$\frac{\bar{C}(0)}{G_c} = \left\{\frac{1}{Sk} - 1 + \frac{\mathscr{U}\gamma^2}{MG_c}\right\}\delta, \tag{6.12}$$

and

$$\bar{u}(z), \bar{v}(z), \bar{w}(z), \bar{C}(z) \to 0 \quad \text{as} \quad z \to \infty, \tag{6.13}$$

where $G_c = Sc\,\hat{G}_c$ and $\mathscr{U} = Sc\,\hat{\mathscr{U}}$.

6.1. *Squire's transformation*

The above equations (6.1)–(6.5) with boundary conditions (6.8)–(6.13) can be converted to an equivalent set of two-dimensional equations by the appropriate Squire's transformation (see Drazin & Reid 1981). We set

$$\tilde{\alpha} = \gamma, \quad \tilde{\alpha}\tilde{u} = \alpha\bar{u} + \beta\bar{v}, \quad \tilde{w} = \bar{w}, \quad \tilde{p}/\tilde{\alpha} = \bar{p}/\alpha, \quad \tilde{\alpha}\tilde{C} = \alpha\bar{C}, \quad \tilde{\alpha}\tilde{\delta} = \alpha\delta, \tag{6.14}$$

and define a new Reynolds number $\tilde{Re}$ by

$$\tilde{Re} = \alpha\,Re/\tilde{\alpha}. \tag{6.15}$$

Then (6.1)–(6.15) become

$$[\mathrm{D}^2 + \mathrm{D} - \tilde{\alpha}^2 - \mathrm{i}\tilde{\alpha}\tilde{Re}(U_0 - c)]\,\tilde{u}(z) = \tilde{Re}\,\tilde{w}(z)\,U_0'(z) + \mathrm{i}\tilde{\alpha}\tilde{Re}\,\tilde{p}(z), \tag{6.16}$$

$$[\mathrm{D}^2 + \mathrm{D} - \tilde{\alpha}^2 - \mathrm{i}\tilde{\alpha}\tilde{Re}(U_0 - c)]\,\tilde{w}(z) = \tilde{Re}\,\mathrm{D}\tilde{p}(z), \tag{6.17}$$

$$i\tilde{\alpha}\tilde{u}(z) + D\tilde{w}(z) = 0, \tag{6.18}$$

$$[D^2 + Sc\,D - \tilde{\alpha}^2 - i\tilde{\alpha}\,\tilde{R}e\,Sc\,(U_0 - c)]\,\tilde{C}(z) = \tilde{R}e\,Sc\,C_0'(z)\,\tilde{w}(z), \tag{6.19}$$

with boundary conditions

$$\tilde{u}(0) = -\tilde{\delta}, \tag{6.20}$$

$$\tilde{w}(0) = 0, \tag{6.21}$$

$$\tilde{\delta}G_c\{i\tilde{\alpha}\,\tilde{R}e\,c - k\,Sc\} + D\tilde{C}(0) - Sc\,(k-1)\,\tilde{C}(0) = 0, \tag{6.22}$$

$$\frac{\tilde{C}(0)}{G_c} = \left\{\frac{1}{Sk} - 1 + \frac{\mathscr{U}\tilde{\alpha}^2}{MG_c}\right\}\tilde{\delta}, \tag{6.23}$$

and

$$\tilde{u}(z), \tilde{w}(z), \tilde{C}(z) \to 0 \quad \text{as} \quad z \to \infty. \tag{6.24}$$

These equations have exactly the same form as (6.1)–(6.5) and (6.8)–(6.13) with $\beta = v = 0$ and they thus define the equivalent two-dimensional problem. It is sufficient therefore to consider only two-dimensional disturbances from which the solutions to the full three-dimensional problem can be obtained merely by reversing the transformation (6.14) and (6.15). Since $\tilde{R}e = Re/(1+\beta^2/\alpha^2)^{\frac{1}{2}}$ is always less than or equal to Re we have a form of Squire's theorem for this problem stating that for fixed Sekerka number it is sufficient to consider only two-dimensional disturbances in order to determine the minimum critical Reynolds number for the shear flow instability. Clearly the Reynolds number will be least when β is zero, hence the most unstable mode occurs in the direction of the free-stream flow.

6.2. *Two-dimensional equations*

In the light of the above we consider only two-dimensional disturbances. Hence we introduce a stream function $\psi(x, z, t)$ in (6.1)–(6.5) and (6.8)–(6.13) such that

$$u(x, z, t) = -\frac{\partial\psi}{\partial z}, \quad w(x, z, t) = \frac{\partial\psi}{\partial x}, \tag{6.25}$$

where

$$\psi(x, z, t) = \phi(z)\exp(i\alpha(x - ct)), \tag{6.26}$$

and after eliminating $\bar{p}(z)$ we obtain

$$[(D^2 - \alpha^2)(D^2 + D - \alpha^2) - i\alpha\,Re\,\{(U_0 - c)(D^2 - \alpha^2) - U_0''\}]\,\phi(z) = 0, \tag{6.27}$$

$$[D^2 + Sc\,D - \alpha^2 - i\alpha\,Re\,Sc\,(U_0 - c)]\,\bar{C}(z) = i\alpha\,Re\,Sc\,C_0'(z)\,\phi(z), \tag{6.28}$$

with boundary conditions

$$\phi(0) = 0, \tag{6.29}$$

$$D\phi(0) = \delta, \tag{6.30}$$

$$\delta G_c\{i\alpha c\,Re - k\,Sc\} + D\bar{C}(0) - Sc\,(k-1)\bar{C}(0) = 0, \tag{6.31}$$

$$\frac{\bar{C}(0)}{G_c} = T(\alpha, Sk)\,\delta, \tag{6.32}$$

and

$$\phi(z), D\phi(z), \bar{C}(z) \to 0 \quad \text{as} \quad z \to \infty, \tag{6.33}$$

where

$$T(\alpha, Sk) = \frac{1}{Sk} - 1 + \frac{\mathscr{U}\alpha^2}{MG_c}. \tag{6.34}$$

Equations (6.27)—(6.33) thus define an eigenvalue problem for c.

7. Asymptotic solution for high Reynolds number

In this section we seek a solution of (6.27), (6.28) and the associated boundary conditions (6.29)–(6.33) for the perturbed flow and solute concentration respectively, in the limit $Re \to \infty$. We proceed in three stages. In the first we consider the perturbed flow, in the second the perturbed concentration and in the final stage we apply the interfacial boundary conditions to obtain an asymptotic form of the dispersion relation.

7.1. *The perturbed flow*

As we have neglected buoyancy effects the modified Orr–Sommerfeld equation (6.27) is decoupled from the perturbed solute concentration. Thus the general form of the solution in the limit $Re \to \infty$ is identical to that of the asymptotic boundary-layer profile obtained by Hughes & Reid (1965). Here we summarize the relevant points of their analysis and refer the reader to Hughes & Reid (1965) and Drazin & Reid (1981) for further details.

These authors showed that the corresponding Rayleigh's equation (in which viscous effects are neglected) has a regular singular point known as the critical point at $z = z_c$ where

$$z_c = -\log(1-c). \tag{7.1}$$

They went on to show that the solution of (6.27) is of the form

$$\phi(z) = a_1 \Phi(z) + a_2 \phi_3(z), \tag{7.2}$$

as $Re \to \infty$, where a_1 and a_2 are constants to be determined from the boundary conditions. The function $\Phi(z)$ is the so-called inviscid solution and is given from Rayleigh's equation as

$$\Phi(z) = \exp\{-\alpha(z-z_c)\}\left\{1-(1-t)F(p+1,q+1;2;1-t)\log(1-t) - \sum_{n=0}^{\infty} A_n(\alpha)\frac{(1-t)^{n+1}}{(n+1)!}\right\} + O(Re^{-1}). \tag{7.3}$$

Here $t = \exp(-z)/(1-c)$,

$$A_n(\alpha) = \frac{\Gamma(p+1+n)\,\Gamma(q+1+n)}{\Gamma(p+1)\,\Gamma(q+1)\,\Gamma(n+1)}\{\psi(p+1+n)+\psi(q+1+n)-\psi(n+1)-\psi(n+2)\}, \tag{7.4}$$

$p = \alpha + (1+\alpha^2)^{\frac{1}{2}}$, $q = \alpha - (1+\alpha^2)^{\frac{1}{2}}$ and $F(a,b;c;x)$ is the hypergeometric function normalized to unity at $x = 1$. The functions $\Gamma(z)$ and $\psi(z)$ are the gamma and digamma functions respectively. The function $\phi_3(z)$ in (7.2) is known as the viscous solution and is given by

$$\phi_3(z) = A_1(\xi, 2) + O(Re^{-\frac{1}{3}}), \tag{7.5}$$

as $Re \to \infty$, where

$$\xi = (z-z_c)/\epsilon, \quad \epsilon = (\mathrm{i}\alpha Re\, U_c^1)^{-\frac{1}{3}}, \tag{7.6}$$

and $A_1(x,p)$ is a generalized Airy function see (Drazin & Reid 1981). We define U_c^n by

$$U_c^n = \frac{\mathrm{d}^n}{\mathrm{d}z^n} U_0(z)|_{z=z_c}.$$

This viscous solution acts on a lengthscale $O(\epsilon)$ ($\sim O(Re^{-\frac{1}{3}})$) about $z = z_c$ and indicates the presence of a critical layer in which viscous effects are important. Below we require the local representation of $\Phi(z)$ in the critical layer, denoted by $\tilde{\Phi}(\xi)$. This is obtained from the rescaling (7.6) applied to the modified Orr–Sommerfeld equation to give

$$\tilde{\Phi}(\xi) = A\left(\epsilon\xi + \tfrac{1}{2}\epsilon^2\xi^2\frac{U_c''}{U_c'}\right) + 1 - \frac{\epsilon U_c''}{U_c'}(B_3(\xi, 2, 1) - H\xi) + O(\epsilon^2), \tag{7.7}$$

where $B_3(\xi, 2, 1)$ is a generalized Airy function, $A = 1 - 2\gamma - \alpha - \psi(p+1) - \psi(q+1)$, and $H = -\gamma + 1 + \log\epsilon + 2\pi i$ is chosen to match $\tilde{\Phi}(\xi)$ with $\Phi(z)$. Here γ is Euler's constant.

7.2. *The perturbed concentration*

We now consider the perturbed concentration. Equations (6.28) and (7.2) give that $\bar{C}(z)$ satisfies

$$[D^2 + Sc\,D - \alpha^2 + i\alpha Re\,Sc\,(c - U_0(z))]\,\bar{C}(z) = i\alpha Re\,Sc\,C_0'(z)\{a_1\Phi(z) + a_2\phi_3(z)\}. \tag{7.8}$$

The general solution is constructed from the homogeneous solution denoted by $\bar{C}_h(z)$ and two particular integrals, denoted by $\bar{C}_I(z)$ and $\bar{C}_V(z)$, corresponding to the inhomogeneous inviscid and viscous flow terms, $\Phi(z)$ and $\phi_3(z)$ respectively, in (7.8).

First we seek a solution of the homogeneous form of (7.8) as a regular perturbation series in Re^{-1}. It is easily shown that this procedure gives $\bar{C}_h \equiv 0$ provided $c - U_0(z) \neq 0$, indicating the presence of a singularity at $z = z_c$. Thus there exists a corresponding critical layer about this point. In this layer solute diffusion balances solute advection and hence we refer to it as the diffusive critical layer. From this consideration we find that the scale of the diffusive critical layer is $O(\epsilon_c)$ where $\epsilon_c = \epsilon Sc^{-\frac{1}{3}}$. Thus we define a new inner variable η by

$$\eta = (z - z_c)/\epsilon_c, \tag{7.9}$$

and note that $\epsilon_c \to 0$ as $Re \to \infty$. We denote the representation of $\bar{C}_h$ in this layer by $\hat{C}_h(\eta)$, in which case the (7.8) gives that

$$\left[\frac{d^2}{d\eta^2} - \eta\right]\hat{C}_h(\eta) = O(\epsilon_c) \quad \text{as} \quad \epsilon_c \to 0, \tag{7.10}$$

hence

$$\hat{C}_h(\eta) = A_1(\eta, 0) + O(\epsilon_c) \quad \text{as} \quad \epsilon_c \to 0. \tag{7.11}$$

Thus

$$\bar{C}_h(z) = A_1\left(\frac{z - z_c}{\epsilon Sc^{-\frac{1}{3}}}, 0\right) + O((Re\,Sc)^{-\frac{1}{3}}) \quad \text{as} \quad Re \to \infty. \tag{7.12}$$

This provides the leading-order approximation to the homogeneous solution of (7.8).

Before considering the particular integrals of (7.8) we shall explain the different lengthscales involved in solving this aspect of the problem. The asymptotic solutions we present are dependent on viscous and diffusive effects in the vicinity of the critical layers that control the onset of instability. As we have demonstrated above, there is a solute diffusion critical layer which acts on a scale $O(\epsilon_c)$ about z_c. However the presence of the inhomogeneous terms in (7.8), corresponding to convective transport due to the perturbed flow, gives rise to two additional scales on which the perturbed solute acts. The first is a scale $O(\epsilon)$ due to the viscous critical layer and the second

is an $O(1)$ lengthscale which defines an outer region. This triple region structure in the general case provides a considerable difficulty in the construction of the particular integrals. We consider the two cases in which we have been able to make progress. The first is the limit $Re \to \infty, Sc \to \infty$, in which case the diffusive critical layer is embedded deep within the viscous critical layer. The second case we consider is $Sc = 1$ where the scale of both the diffusive and viscous critical layers is identical, and hence there are only two regions.

Case 1. The limit $Re \to \infty, Sc \to \infty$

We construct the particular integral in two parts. We first consider $\bar{C}_1$ and then $\bar{C}_V$. Taking the limit $Re \to \infty$ gives that

$$\bar{C}_I(z) = \frac{a_1 C_0'(z)\,\Phi(z)}{c - U_0(z)} + O(Re^{-1}) \quad \text{as} \quad Re \to \infty. \tag{7.13}$$

This represents $\bar{C}_1$ in the outer region. However, clearly this solution is singular as $z \to z_c$ and we seek a new representation of $\bar{C}_1$ in the viscous critical layer. We denote the solution in this region by a tilde, e.g. $\tilde{C}_I(\xi)$. Employing the inner approximations to $\Phi(z)$ given by (7.7) in this inner layer the resulting differential equation for $\tilde{C}_I$ may be solved to yield

$$\begin{aligned}\tilde{C}_I(\xi) = a_1 \Bigg\{ & -\frac{A}{U_c^1}(C_0'(z_c) + \epsilon\xi C_0''(z_c)) - \frac{C_0'(z_c)}{\epsilon\xi U_c^1} \\ & + \frac{C_0'(z_c)}{U_c^1}\left[\frac{1}{\xi^3} + \frac{U_c^2}{U_c^1}\left(\frac{B_3(\xi,2,1)}{\xi} - H + \tfrac{1}{2}\right)\right] - \frac{C_0''(z_c)}{U_c^1}\Bigg\} + O(\epsilon) + O(Sc^{-1}) \\ & \text{as} \quad Re \to \infty, \quad Sc \to \infty. \end{aligned} \tag{7.14}$$

It can be shown that $\bar{C}_I(z)$ and $\tilde{C}_I(\xi)$ match in this limit. However this solution is singular at $\xi = 0$ and we require a new representation of the solution on the scale of the diffusive critical layer, denoted by $\hat{C}_I(\eta)$, in order to allow solute diffusion to act. Thus we rescale (7.8) using (7.9) and solve the resulting differential equation to obtain

$$\begin{aligned}\hat{C}_I(\eta) = a_1 \Bigg\{ & -\frac{A}{U_c^1}(C_0'(z_c) + \epsilon_c \eta C_0''(z_c)) + \frac{C_0'(z_c)}{\epsilon_c U_c^1} B_3(\eta, 0) \\ & + \frac{C_0'(z_c)\,U_c^2}{(U_c^1)^2}\Big(Sc^{\frac{1}{3}} e^{-\frac{4\pi i}{3}} \tfrac{1}{3}\Gamma(\tfrac{2}{3}) B_3(\eta,0) + \tfrac{1}{3}(\log 3 - \gamma) + \pi i - H + \tfrac{1}{10}B_3(\eta,-5) - \tfrac{1}{2}\eta B_3(\eta,0)\Big) \\ & - \frac{C_0''(z_c)}{U_c^1} - Sc\,\frac{C_0'(z_c)}{2U_c^1} B_3(\eta,-2)\Bigg\} + O(\epsilon_c) \quad \text{as} \quad \epsilon_c \to 0. \end{aligned} \tag{7.15}$$

Again $\hat{C}_I(\eta)$ matches with $\tilde{C}_I(\xi)$ as $Re \to \infty, Sc \to \infty$ and the solution is bounded at $\eta = 0$ as required.

We now consider the viscous particular integral. In the same way as before

$$\bar{C}_V(z) = \frac{a_2 C_0'(z)\,\phi_3(z)}{c - U_0(z)} \tag{7.16}$$

represents this particular integral in the outer region. Again this is singular at $z = z_c$ and we seek a new description of $\bar{C}_V$ in the viscous critical layer. Applying the appropriate rescaling of (7.8) and taking the limit $Sc \to \infty$ we obtain

$$\tilde{C}_V(\xi) = -\frac{a_2 C_0'(z_c) A_1(\xi, 2)}{\epsilon\xi U_c^1} + O(Sc^{-1}) + O(\epsilon) \quad \text{as} \quad Re \to \infty, Sc \to \infty. \tag{7.17}$$

This clearly matches with the outer representation $\bar{C}_V(z)$ given in (7.16). However $\tilde{C}_V(\xi)$ is singular as $\xi \to 0$ and we again seek the solution in the diffusive critical layer in a similar way to before, which gives

$$\hat{C}_V(\eta) = \frac{a_2 C_0'(z_c) A_1(0,2) B_3(\eta,0)}{\epsilon_c U_c'} + O(\epsilon_c) + O(\epsilon) \quad \text{as} \quad Re \to \infty, Sc \to \infty. \tag{7.18}$$

This is bounded as $\eta \to 0$ and can be shown to match with the solution in the viscous critical layer (7.17). Thus in the limit $Re \to \infty, Sc \to \infty$ the leading-order approximation to the solution of (7.8) is taken to be

$$\bar{C}(z) = \frac{C_0'(z)}{(c - U_0(z))}\{a_1 \Phi(z) + a_2 \phi_3(z)\} + a_3 A_1\left(\frac{z - z_c}{\epsilon Sc^{-\frac{1}{3}}}, 0\right). \tag{7.19}$$

We now employ the boundary conditions (6.29)–(6.32) along with the approximations (7.2) and (7.19) to $\phi(z)$ and $\bar{C}(z)$ to obtain at leading order

$$\left(\frac{\Phi(0)}{\Phi'(0)} - \frac{\phi_3(0)}{\phi_3'(0)}\right)\left(\frac{1}{c} + f(\alpha, c, Re, Sk)\right) = 0, \tag{7.20}$$

where

$$f(\alpha, c, Re, Sk) = \mathrm{i}\alpha c\, Re - k\, Sc - \left(\frac{1}{Sk} - 1 + \frac{\mathscr{U}\alpha^2}{MG_c}\right)\left(Sc\,(k-1) - \frac{1}{z_c F(Y Sc^{\frac{1}{3}}, 0)}\right), \tag{7.21}$$

and $Y = z_c(\alpha Re\, U_c')^{\frac{1}{3}}$. Here $F(z,p)$ is the generalized, order-p Tietjens function (see Drazin & Reid 1981). There are two solution branches to this dispersion relation. The first, given by

$$\frac{\Phi(0)}{\Phi'(0)} - \frac{\phi_3(0)}{\phi_3'(0)} = 0, \tag{7.22}$$

is that obtained by Hughes & Reid (1965) for the instability of the asymptotic suction profile, and so corresponds to a rigid, plane interface. The second,

$$\frac{1}{c} + f(\alpha, c, Re, Sk) = 0, \tag{7.23}$$

can be identified with the morphological mode of instability.

We have solved numerically the relation (7.22). The marginal curve in $(Re^{\frac{1}{3}}, \alpha)$-space is shown in figure 11 and the corresponding wave speed c is given as a function of the wavenumber α in figure 12. We determined the minimum critical Reynolds number Re_{crit} and the corresponding critical values of α_{crit} and c_{crit}. These were $Re_{\text{crit}} = 46095$, $\alpha_{\text{crit}} = 0.1592$, $c_{\text{crit}} = 0.1564$, and compare very favourably with those found by Lakin & Reid (1982) and L. M. Mack (unpublished) (see Drazin & Reid 1981) who found $Re_{\text{crit}} = 46093$, $\alpha_{\text{crit}} = 0.159$, $c_{\text{crit}} = 0.1564$ and $Re_{\text{crit}} = 47047$, $\alpha_{\text{crit}} = 0.1630$, $c_{\text{crit}} = 0.1559$ respectively.

We performed a numerical solution of the full system of differential equations and boundary conditions (6.27)–(6.33) by a similar method to that described in §5. Our results are displayed in table 2 for the model lead alloy data given in table 1 but with $Sc = 5$. We see that over the range of Sekerka numbers between 10^{-3} and 2 the critical values of Re, α, and c are almost constant. This confirms the above analysis that indicates that the shear flow mode of instability is unaffected by the presence of the freezing interface for high Schmidt numbers. The quantitative disparity

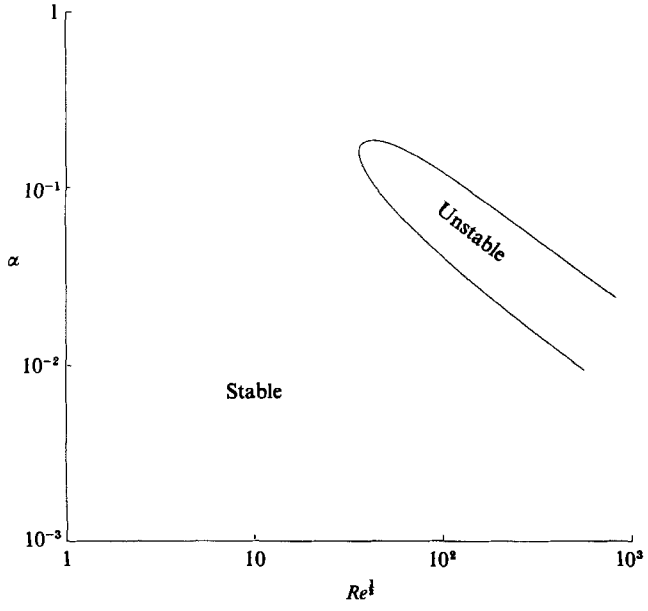

FIGURE 11. The marginal stability curve obtained from (7.22) corresponding to the shear mode of instability.

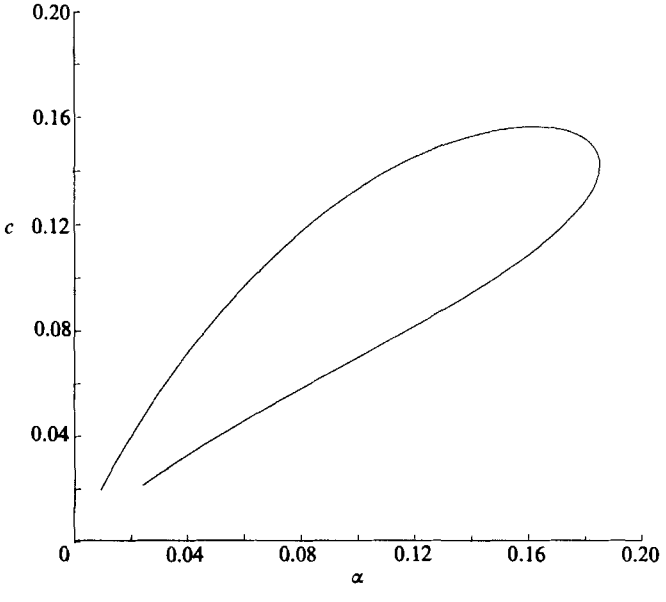

FIGURE 12. The wave speed c along the marginal curve of figure 11.

between the asymptotic results and the numerical solution of the governing equations can be attributed to the neglect of the D^3 operation in the approximations to the Orr–Sommerfeld equation, as was remarked by Lakin & Reid (1982).

A numerical solution of the morphological branch given by (7.23) yields unrealistic behaviour. In our numerical solution of the full set of differential equations described in §5 the wave speed (scaled with respect to the solute field scaling) on the morphological branch is order one as the Reynolds number increases. Thus on the

Sekerka number *Sk*	Reynolds number *Re*	Wavenumber α	Wave speed c
10^{-3}	54379	0.1555	0.1499
10^{-2}	54383	0.1555	0.1499
4×10^{-2}	54381	0.1555	0.1499
10^{-1}	54366	0.1550	0.1498
1	54329	0.1550	0.1499
2	54324	0.1550	0.1499

Non-dimensional constants: Schmidt number, $Sc = 5$; Partition coefficient, $k = 0.3$; Liquidus slope, $M = 0.38804\times10^{-4}$; Capillarity parameter, $\mathscr{U} = 0.6852\times10^{-8}$.

TABLE 2. Table of parameters at onset of shear flow mode of instability for a Schmidt number of 5

shear flow scaling the wave speed becomes very small as the Reynolds number becomes large. This results in the two critical layers becoming adjacent to the solid–liquid interface and hence the outer approximations used to derive (7.20) will not be appropriate.

Case 2. Sc = 1

As noted above, in this case the viscous and diffusive critical layers act on the same scale. Again we take the inviscid solute particular integral to be (7.13) as $Re\to\infty$. But now the representation in the common critical layer (which we denote by $\tilde{C}(\xi)$) is found to be

$$\tilde{C}_1(\xi) = a_1\Bigg\{-\frac{A}{U_c^1}(C_0'(z_c)+\epsilon\xi C_0''(z_c))+\frac{C_0'(z_c)}{\epsilon U_c^1}B_3(\xi,0)-\frac{C_0'(z_c)}{U_c^1} + \frac{C_0'(z_c)}{U_c^1}\Bigg[-\tfrac{1}{2}B_3(\xi,-2)+\frac{U_c^2}{U_c^1}\{1+B_3(\xi,1,1)-H-\tfrac{1}{2}\xi B_3(\xi,0)+\tfrac{1}{10}B_3(\xi,-5)\}\Bigg]\Bigg\}+O(\epsilon) \quad \text{as} \quad \epsilon\to0, \tag{7.24}$$

which matches with the outer form of the inviscid particular integral (7.13).

We find that the viscous particular integral is given by

$$\tilde{C}_V(\xi) = -\frac{C_0'(z_c)\,a_2 A_1(\xi,1)}{\epsilon U_c^1}. \tag{7.25}$$

These results give the following approximation to $\bar{C}(z)$:

$$\bar{C}(z) = \frac{a_1 C_0'(z)}{(c-U_0(z))}\Phi(z)-\frac{a_2 C_0'(z_c)}{\epsilon U_c^1}A_1\left(\frac{z-z_c}{\epsilon},1\right)+a_3A_1\left(\frac{z-z_c}{\epsilon},0\right) \quad \text{as} \quad Re\to\infty. \tag{7.26}$$

Further, employing (7.2) as the approximation to $\phi(z)$ and applying the interfacial boundary conditions (6.28)–(6.31) gives the following approximation to the dispersion relation:

$$\frac{\Phi(0)}{\Phi'(0)} = \frac{-z_c F(Y,2)\left[\dfrac{1}{c}+f(\alpha,c,Re,Sk)\right]}{\left[\dfrac{1}{z_c}\left(\dfrac{1}{F(Y,1)}-\dfrac{1}{F(Y,0)}\right)+z_c F(Y,2)\left(1-c+\dfrac{c}{z_c F(Y,0)}\right)+f(\alpha,c,Re,Sk)\right]}. \tag{7.27}$$

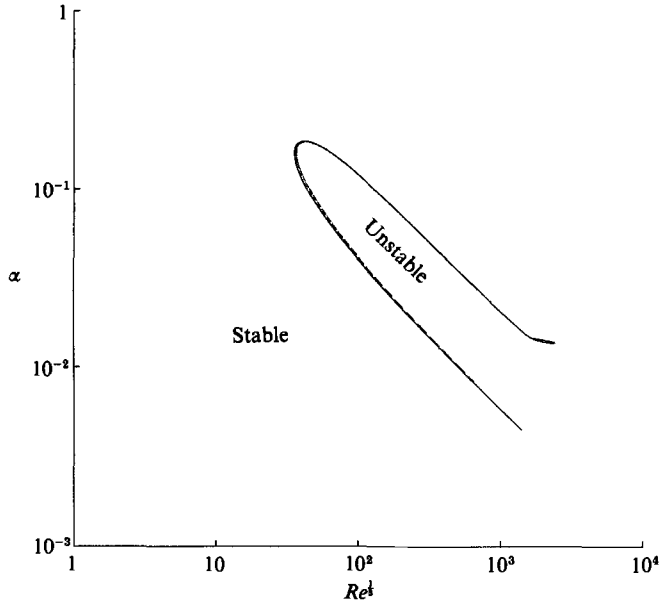

FIGURE 13. Marginal stability curves obtained from (7.27) for Sekerka numbers of 10^{-3} (solid line) and 2 (broken line) when the Schmidt number is unity. The material parameters are for the lead/tin alloy given in table 1 with a far-field concentration of 0.01 wt % and a growth speed of 10^{-3} cm/s.

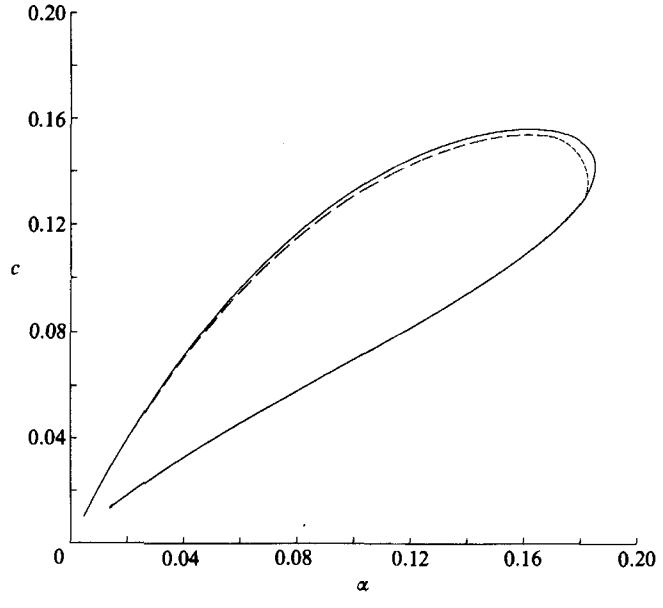

FIGURE 14. The wave speed along the marginal curves of figure 13.

In the limit $Sk \to 0$ this expression becomes

$$\frac{\Phi(0)}{\Phi'(0)} = -z_c F(Y, 2), \tag{7.28}$$

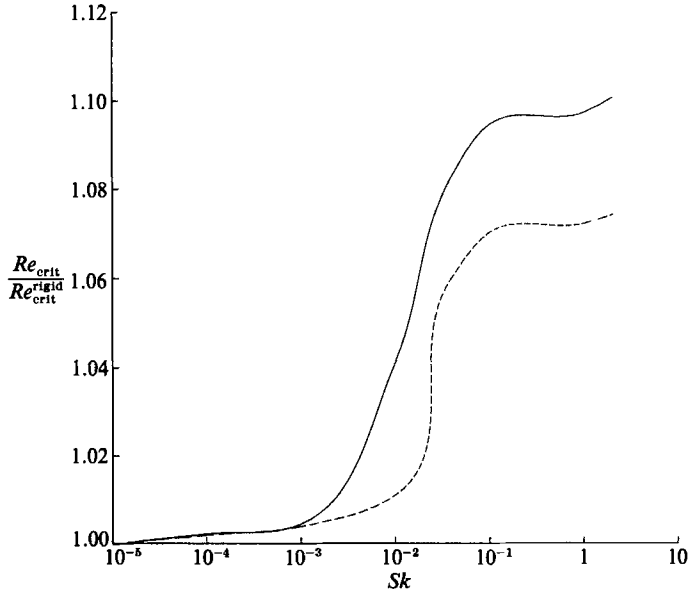

FIGURE 15. A comparison of the critical Reynolds number obtained from the asymptotic prediction, via (7.27), and a numerical solution of the eigenvalue problem, given by (6.27)–(6.33), for the case of Schmidt number $Sc = 1$. The solid and broken lines correspond to the asymptotic and numerical results respectively. Each has been scaled with respect to its value at $Sk = 0$ which corresponds to a rigid interface. The material parameters are those of the lead/tin alloy given in table 1 with a far-field concentration of 0.01 wt % and a growth speed of 10^{-3} cm/s.

which is the result of Hughes & Reid (1965) for a rigid planar interface and is equivalent to (7.22). This is to be expected because a small Sekerka number corresponds to a large temperature gradient in which case the liquidus condition constrains the interface deflection to be small. We have numerically solved the approximate dispersion relation (7.27) to obtain the marginal curve in $(Re^{\frac{1}{3}}, \alpha)$-space for fixed values of the Sekerka number. In figures 13 and 14 we present our results for the lead–tin system for the cases $Sk = 10^{-3}$ and $Sk = 2$. Further, in figure 15 we plot the critical Reynolds number derived from (7.27) as well as its values obtained from the numerical solution of the full differential equations. In each case the Reynolds number has been scaled by a factor to ensure that at zero Sekerka number they are both unity. This is so that we may compare the asymptotic and numerical solutions, which differ for the reasons discussed above. Clearly the results are in good qualitative agreement and indicate a stabilization of the shear instability with increasing Sekerka number.

8. Conclusions

In §§4 and 5 we have considered the effect of a shear flow on the morphological stability of the planar interface of a freezing binary alloy. A linear stability analysis shows that modes with wave vectors perpendicular to the flow are unaffected. However, the asymptotic analysis presented in §4 for the realistic limit $Sc \to \infty$ shows that the main effect of the flow is to cause the appearance of *travelling waves along* the interface with a speed proportional to the Reynolds number. The wave speed may be positive or negative and its sign is dependent solely upon the wavenumber

of the disturbance and the partition coefficient, as indicated in figure 4. A lesser effect of the flow is to alter the value of the critical Sekerka number by an amount that is proportional to the square of the Reynolds number and is further dependent on the partition coefficient and wavenumber. These last two quantities solely determine whether these modes are stabilized or destabilized. For typical alloys the critical wavenumber is greater than one and thus our analysis predicts that the modes with wave vectors parallel to the flow are stabilized and hence the most unstable modes are those perpendicular to the flow.

The numerical calculations presented in §5 indicate that, for the model lead/tin alloy, modes parallel to the flow direction are further stabilized with increasing Reynolds number; the band of wavenumbers close to the critical Sekerka number narrows and the critical wavenumber increases.

In §§6 and 7 we considered the effect of a freezing planar interface on the hydrodynamic stability of the model boundary-layer flow. In contrast to the morphological mode of instability we have shown, from an extension of Squire's theorem to this situation, that disturbances with wave vectors parallel to the flow are always the most unstable. Both the numerical calculations and the asymptotic results for large Reynolds number indicate that the hydrodynamic instability is only weakly affected. We attribute this to the mismatch in lengthscales between the solute and momentum boundary layers. However for the special case of Schmidt number unity there is a stronger coupling resulting in a modest stabilization.

The authors wish to express their thanks to Dr S. R. Coriell, Dr G. B. McFadden and Professor D. T. J. Hurle for helpful discussion relating to this work. One of us, S. A. F., gratefully acknowledges the receipt of an SERC grant.

Appendix. The functions $f_1(\hat{\gamma}, k)$, $f_2(\hat{\gamma}, k)$ and $d_1(\hat{\gamma}, k)$

The functions $f_1(\hat{\gamma}, k)$ and $f_2(\hat{\gamma}, k)$ are given by

$$f_1(\hat{\gamma}, k) = \frac{1}{\hat{\gamma}^3}\left\{2 + 2(2\hat{\gamma}+1)\,H^*(\hat{\gamma}, k) - \frac{3}{\hat{\gamma}}(2\hat{\gamma}+1)^2\right\}, \tag{A 1}$$

$$f_2(\hat{\gamma}, k) = \frac{1}{\hat{\gamma}^2}\left\{H^*(\hat{\gamma}, k) - \frac{3}{\hat{\gamma}}(2\hat{\gamma}+1)\right\}, \tag{A 2}$$

where $H^*(\hat{\gamma}, k)$ is given as in (4.13).

The function $d_1(\hat{\gamma}, k)$ is given by

$$d_1(\hat{\gamma}, k) = -\frac{1}{2R}\left\{\frac{3a_3(\hat{\gamma}, k)}{4R^3} + \frac{a_2(\hat{\gamma}, k)}{2R^2} + \frac{a_1(\hat{\gamma}, k)}{2R} + a_0(\hat{\gamma}, k)\right\}, \tag{A 3}$$

where

$$a_0(\hat{\gamma}, k) = H(\hat{\gamma}, k)\,\mathscr{C}_1(\hat{\gamma}, k), \tag{A 4}$$

$$a_1(\hat{\gamma}, k) = -\mathscr{C}_1(\hat{\gamma}, k) + \frac{kH(\hat{\gamma}, k)}{(k-\frac{1}{2}+R)}\mathscr{C}_3(\hat{\gamma}, k), \tag{A 5}$$

$$a_2(\hat{\gamma}, k) = \frac{k}{(k-\frac{1}{2}+R)}(H(\hat{\gamma}, k)\,\mathscr{C}_2(\hat{\gamma}, k) - \mathscr{C}_3(\hat{\gamma}, k)), \tag{A 6}$$

$$a_3(\hat{\gamma}, k) = \frac{-k\mathscr{C}_2(\hat{\gamma}, k)}{(k-\frac{1}{2}+R)}; \tag{A 7}$$

and
$$\mathscr{C}_1(\hat{\gamma},k)=\frac{1}{(k-\frac{1}{2}+R)}\left\{H^*(\gamma,k)\left[1-\frac{k}{2R(k-\frac{1}{2}+R)}\right]\right.$$
$$\left.-\left[\frac{(k+\hat{\gamma})(2\hat{\gamma}+1)}{\hat{\gamma}^2}-\frac{1}{\hat{\gamma}}-\frac{k}{4R^2(k-\frac{1}{2}+R)}\right]\right\}, \quad \text{(A 8)}$$

$$\mathscr{C}_2(\hat{\gamma},k)=\frac{1}{4R}, \quad \text{(A 9)}$$

$$\mathscr{C}_3(\hat{\gamma},k)=\frac{1}{2R}\left\{\frac{1}{2R}-H^*(\hat{\gamma},k)\right\}. \quad \text{(A 10)}$$

REFERENCES

Brattkus, K. & Davis, S. H. 1988*a* Flow induced morphological instabilities: the rotating disk. *J. Cryst. Growth* **87**, 385–396.

Brattkus, K. & Davis, S. H. 1988*b* Flow induced morphological instabilities: stagnation point flows. *J. Cryst. Growth* **89**, 423–427.

Chiarulli, P. & Freeman, J. C. 1948 *Tech. Rep. F-TR-1197-IA*. Headquarters Air Material Command, Dayton.

Coriell, S. R., McFadden, G. B., Boisvert, R. F. & Sekerka, R. F. 1984 Effect of a forced Couette flow on coupled convective and morphological instabilities during unidirectional solidification. *J. Cryst. Growth* **69**, 15–22.

Coriell, S. R., McFadden, G. B. & Sekerka, R. F. 1985 Cellular growth during directional solidification. *Ann. Rev. Mater. Sci.* **15**, 119–145.

Coriell, S. R. & Sekerka, R. F. 1981 Effect of convective flow on morphological stability. *Physicochem. Hydrodyn.* **2**, 281–293.

Delves, R. T. 1968 Theory of stability of a solid–liquid interface during growth from stirred melts. *J. Cryst. Growth* **3**, **4**, 562–568.

Delves, R. T. 1971 Theory of stability of a solid–liquid interface during growth from stirred melts II. *J. Cryst. Growth* **8**, 13–25.

Drazin, P. G. & Reid, W. H. 1981 *Hydrodynamic Stability*. Cambridge University Press.

Fank, Q. T., Glicksman, M. E., Coriell, S. R., McFadden, G. B. & Boisvert, R. F. 1985 Convective influence on the stability of a cylindrical solid–liquid interface. *J. Fluid Mech.* **151**, 121–140.

Glicksman, M. E., Coriell, S. R. & McFadden, G. B. 1986 Interaction of flows with the crystal–melt interface. *Ann. Rev. Fluid Mech.* **18**, 307–335.

Hocking, L. M. 1975 Non-linear instability of the asymptotic suction velocity profile. *Q. J. Mech. Appl. Maths* **28**, 341–353.

Hughes, T. H. & Reid, W. H. 1965 On the stability of the asymptotic suction boundary-layer profile. *J. Fluid Mech.* **23**, 715–735.

Keller, H. B. 1976 *Numerical Solution Of Two Point Boundary Value Problems*. Philadelphia: SIAM.

Lakin, W. D. & Reid, W. H. 1982 Asymptotic analysis of the Orr–Sommerfeld suction boundary layer flows. *Q. J. Mech. Appl. Maths* **35**, 69–89.

McCartney, D. G. & Hunt, J. D. 1981 Measurement of cell and primary dendrite arm spacing in directionally solidified aluminium alloys. *Acta Metall.* **29**, 1851–1863.

McFadden, G. B., Coriell, S. R. & Alexander, J. I. D. 1988 Hydrodynamic and free boundary instabilities during crystal growth: the effect of a plane stagnation point flow. *Commun. Pure Appl. Maths* **41**, 683–706.

McFadden, G. B., Coriell, S. R., Boisvert, R. F., Glicksman, M. E. & Fang, Q. T. 1984 Morphological stability in the presence of fluid flow in the melt. *Metall. Trans.* **15A**, 2117–2124.

Morris, L. R. & Winegard, W. C. 1969 The development of cells during the solidification of a dilute Pb–Sn alloy. *J. Cryst. Growth* **5**, 361–375.

MULLINS, W. W. & SEKERKA, R. F. 1964 Stability of a planar interface during solidification of a dilute binary alloy. *J. Appl. Phys.* **35**, 444–451.

NG, B. S. & REID, W. H. 1980 On the numerical solution of the Orr–Sommerfeld problem: asymptotic initial conditions for shooting methods. *J. Comp. Phys.* **38**, 275–293.

RUTTER, J. W. & CHALMERS, B. 1953 A prismatic substructure formed during solidification of metals. *Can. J. Phys.* **31**, 15–39.

SCOTT, M. R. & WATTS, H. A. 1975 SUPORT: a computer code for two-point boundary-value problems via orthonormalization. *SAND* 75-0198. Albuquerque: Sandia Laboratories.

TILLER, W. A., RUTTER, J. W., JACKSON, K. A. & CHALMERS, B. 1953 The redistribution of solute atoms during the solidification of metals. *Acta Metall.* **1**, 428–437.

WOLLKIND, D. J., OULTON, D. B. & SRIRANGANATHAN, R. 1984 A nonlinear stability analysis of a model equation for alloy solidification. *J. Phys. Paris* **45**, 505–516.

WOLLKIND, D. J. & SEGEL, L. A. 1970 A nonlinear stability analysis of the freezing of a dilute binary alloy. *Phil. Trans. R. Soc. Lond.* A **268**, 351–380.